24. R. F. Howe, *Colloids and Surf. A: Physicochem. Eng. Aspects* **72**, 353 (1993).
25. ——, *Adv. Colloid Interface Sci.* **18**, 1 (1982).
26. An application of published activation energies (*24*) to diffusion time scales in the martian soil is inappropriate because there is limited information on the effects of grain boundaries on the mobility of the O_2^- radicals. We believe that migration of surface-generated O_2^- across soil grains to a depth of 10 cm or more is certainly possible on geologic time scales, but more work is necessary to characterize the mobility of this species in a granular material.
27. J. H. Lunsford, *Am. Chem. Soc. Sympos. Ser.* **248**, 127 (1984).
28. A. M. Gasymov *et al.*, *Kinet. Katal.* **25**, 358 (1984).
29. F. A. Cotton, G. Wilkinson, P. L. Gaus, *Basic Inorganic Chemistry* (Wiley, New York, 1995), pp. 435–443.
30. V. I. Oyama, B. J. Berdahl, G. C. Carle, *Nature* **265**, 110 (1977).
31. E. B. Ballou, P. C. Wood, T. Wydeven, M. E. Lehwalt, R. E. Mack, *Nature* **271**, 644 (1978).
32. The UV lamp used in the experiments has an output of 10^{-3} W/cm². The ~2 cm² of sample cross section exposed to the lamp corresponds to a capture of ~10^{15} photons per s at a wavelength of 254 nm.
33. W. R. Kuhn and S. K. Atreya, *J. Mol. Evol.* **14**, 57 (1979).
34. The long wavelength cutoff for photons capable of generating oxygen radicals on martian mineral grains is inherently uncertain because the band gap for mobilizing electrons depends on the specific content of impurities. However, the use of 3500 Å for this order-of-magnitude estimate is reasonable.
35. The concentration of oxygen in the martian troposphere (~0.13% by volume) is high enough to allow more than 10^{18} collisions with each cm² of soil surface area each second. This value is at least 10 orders of magnitude greater than the total number of oxygen radicals we expect to form on Mars in 1 s; therefore, we conclude that the oxygen abundance is not a limiting factor.
36. D. L Perry, *Instrumental Surface Analysis of Geologic Materials* (VCH, New York, 1990).
37. C. L. Johnston, M. E. Gunter, C. R. Knowles, *Gems and Gemology* **27**, 220 (1991).
38. P. R. Christensen *et al.*, *Science* **279**, 1692 (1998).
39. J. L. Bandfield, V. E. Hamilton, P. R Christensen, *Science* **287**, 1626 (2000).
40. N. H. Horowitz, *To Utopia and Back: The Search for Life in the Solar System* (Freeman, New York, 1986), p. 136.
41. This work was performed at the Jet Propulsion Laboratory, California Institute of Technology, under contract to the National Aeronautics and Space Administration.

5 May 2000; accepted 2 August 2000

Osmium Isotopic Evidence for Mesozoic Removal of Lithospheric Mantle Beneath the Sierra Nevada, California

Cin-Ty Lee[1]*, Qingzhu Yin,[1] Roberta L. Rudnick,[1]† John T. Chesley,[2] Stein B. Jacobsen[1]

Thermobarometric and Os isotopic data for peridotite xenoliths from late Miocene and younger lavas in the Sierra Nevada reveal that the lithospheric mantle is vertically stratified: the shallowest portions (<45 to 60 kilometers) are cold (670° to 740°C) and show evidence for heating and yield Proterozoic Os model ages, whereas the deeper portions (45 to 100 kilometers) yield Phanerozoic Os model ages and show evidence for extensive cooling from temperatures >1100°C to 750°C. Because a variety of isotopic evidence suggests that the Sierran batholith formed on preexisting Proterozoic lithosphere, most of the original lithospheric mantle appears to have been removed before the late Miocene, leaving only a sliver of ancient mantle beneath the crust.

Lithospheric removal, in the form of detachment, foundering, or peeling away of the lithospheric mantle with or without lower crust into the convecting mantle, has been predicted by various geodynamic models (*1–4*) and may have important geochemical implications (*5*, *6*). For lack of a better term, these forms of lithospheric removal are referred to here as "delamination" in order to distinguish them from lithospheric removal associated with extension or upwelling-induced erosion (*7*). Finding direct evidence for delamination is difficult: although delamination is predicted to cause increased magmatism, changes in magmatic composition, high elevations, high rates of uplift, and low P_n velocities (*8–12*), these phenomena can also be explained by extension or active upwelling.

The extinct Mesozoic Sierra Nevada arc is one place where removal of the underlying subcontinental lithospheric mantle (SCLM) has been proposed. The Sierra Nevada is characterized by high elevations, low P_n velocities (*9–11*), and variable xenolith assemblages (*12*). The latter have been interpreted to reflect delamination of an eclogitic lower crust (*12*). Because the Sierra Nevada was built on Proterozoic lithosphere, as evidenced by radiogenic Sr and ~1.6 Ga Sm-Nd model ages in batholithic rocks (*13*, *14*), the present Sierran SCLM should be young if delamination occurred during or after arc formation. However, many Cenozoic basalts [18 million years ago (Ma) to the present] erupted throughout the Sierra Nevada and western edge of the Great Basin have high $^{87}Sr/^{86}Sr$, low $^{143}Nd/^{144}Nd$, and low $^{3}He/^{4}He$ ratios, which collectively have been interpreted to derive from ancient [>0.8 billion years ago (Ga)] lithospheric mantle (*15–17*). Here, we use Os isotopes and major-element partitioning between mineral phases (thermobarometry) in lithospheric mantle xenoliths to determine the age of the SCLM and to estimate their pressure and temperature conditions, thereby allowing us to evaluate the extent and nature of SCLM removal.

The Re-Os isotopic system is the most robust method of dating the formation of SCLM (*18–21*), which is stabilized by conductive cooling and partial melting in the uppermost mantle. The latter produces a buoyant, refractory residue, having a low Re/Os ratio (Re is incompatible and Os is compatible in the residue during partial melting), which correlates with other indicators of fertility such as Ca and Al. Such a residue, if isolated in the SCLM, will develop low time-integrated $^{187}Os/^{188}Os$ relative to the convecting mantle. Ideally, one can use the Re/Os ratio of a peridotite along with its $^{187}Os/^{188}Os$ ratio to determine a Re-Os model age by extrapolating back to the point in time to where the peridotite's $^{187}Os/^{188}Os$ ratio intersects the mantle evolution curve (*21*). However, a number of factors may lead to Re/Os ratios that are not truly representative of the residual peridotite (*22*). In these cases, there are two other ways of determining model ages. "Re depletion" model ages (T_{RD}) assume that Re/Os is zero, and therefore yield minimum ages. For the most refractory peridotites, T_{RD} ages approximate the time of the melting event. Alternatively, major elements such as Ca and Al can be used as proxies for Re/Os, with the age of the melting event inferred from the $^{187}Os/^{188}Os$ intercept at Al_2O_3 = 0 (*23*). The Mg# [Mg/(Mg + Fe)] may also be used as an inverse proxy (*23*).

The large contrast between the age of the original Sierran lithosphere (~1.6 Ga) and the age of its hypothetical removal (Mesozoic and younger) is within the resolution of the

[1]Department of Earth and Planetary Sciences, Harvard University, 20 Oxford Street, Cambridge, MA 02138, USA. [2]Department of Geological Sciences, Gould-Simpson Building, Building 77, University of Arizona, Tucson, AZ 85712, USA.

*To whom correspondence should be addressed. E-mail: ctlee@eps.harvard.edu

†Present address: Department of Geology, University of Maryland, College Park, MD 20742, USA.

Re-Os isotopic system. Thus, if Proterozoic SCLM persists, it will be characterized by unradiogenic $^{187}Os/^{188}Os$ in the most refractory samples [e.g., <0.122 (*24*)], and if it has been recently removed and replaced by asthenospheric mantle, radiogenic $^{187}Os/^{188}Os$ is expected [0.122 to 0.130 (*20*)].

We selected 13 fresh peridotite xenoliths for Os isotopic analyses (*25*). The xenoliths derive from a late Miocene (8 Ma) diatreme (Big Creek) and a Pleistocene (0.115 Ma) basalt flow (Oak Creek) from the central and eastern Sierras, respectively [(*26*) and Fig. 1]. Big Creek peridotites derive from depths between 35 and 100 km and can be divided into a shallow group (<45 to 60 km) and a deeper group (45 to 100 km); the former shows evidence for heating; the latter shows evidence for cooling (Fig. 2). The shallow group consists of spinel peridotites, which originated from depths less than ~45 to 60 km, based on the absence of garnet (*27*). These peridotites contain orthopyroxenes that are either homogeneous or show CaO-enriched rims. Core equilibration temperatures range between ~670° and 740°C, whereas the higher Ca rims yield temperatures up to 900°C (*28*). The deeper group consists of both garnet and spinel peridotites, all of which contain orthopyroxenes with high CaO cores (up to 0.8 weight %) and low CaO rims (0.18 weight %). This reverse zoning reflects cooling from >1100°C to 700° to 800°C (*28*). Pressures of equilibration for the garnet-bearing samples are between 2.2 and 3.2 GPa, or depths of ~66 and 100 km, respectively (*28*, *29*). Oak Creek peridotites are exclusively spinel peridotites derived from depths shallower than 45 km, were hot (1000° to 1100°C), and have homogeneous mineral compositions (*12*, *28*).

The Big Creek peridotites exhibit a wide range in bulk compositions (Table 1), with olivine Mg# ranging from 0.886 to 0.915 and clinopyroxene Na_2O ranging from 0.46 to 1.6 weight % (*30*). In contrast, the Oak Creek peridotites exhibit a narrower range in bulk compositions, with olivine Mg# between 0.894 and 0.900 and clinopyroxene Na_2O between 1.0 and 1.8. Collectively, these mineral compositions reflect variable degrees of melt extraction from a fertile precursor (Mg# ≈ 0.885; clinopyroxene Na_2O ≈ 1.9 weight %).

The deep Big Creek peridotites and all of the Oak Creek peridotites have Os isotopic compositions (0.1263 to 0.1296 and 0.1235 to 0.1309, respectively) that lie within the range of modern convecting mantle [0.122 to 0.130 (*20*)] (Fig. 3). The two shallow peridotites from Big Creek have unradiogenic compositions (0.1219 and 0.1163, T_{RD} = 1.0 and 1.8 Ga, respectively), and one deep peridotite from Big Creek has a significantly superchrondritic composition (0.1507).

Radiogenic $^{187}Os/^{188}Os$ in the most refractory of the deep Big Creek peridotites is strong evidence that the melting event that gave rise to these compositions was relatively recent (*31*), and thus, these samples probably represent young (Phanerozoic) additions to the SCLM. In contrast, the unradiogenic, shallow samples from Big Creek (BC98-2 and P-2 in Table 1) appear to derive from ancient (Proterozoic) lithosphere. The $^{187}Os/^{188}Os$ of the Oak Creek peridotites do not constrain the timing of lithospheric formation, because their more fertile compositions allow for both ancient and recent melt depletion events. For example, one Oak Creek sample, OK98-9, has a somewhat refractory composition (olivine Mg# = 0.900 and clinopyroxene Na_2O = 1.04) and radiogenic $^{187}Os/^{188}Os$ (0.1297), suggesting a recent melt extraction event, whereas one fertile peridotite has unradiogenic $^{187}Os/^{188}Os$ (0.1235), giving a Re depletion age of 1100 Ma.

Thermobarometric and isotopic data thus allow us to determine the age and thermal structure of the central Sierran SCLM at the time the xenoliths were sampled. Original SCLM was removed below ~45 to 60 km and replaced by asthenospheric mantle sometime before 8 Ma (age of Big Creek diatreme). This mantle subsequently cooled from near-adiabatic to near-lithospheric tem-

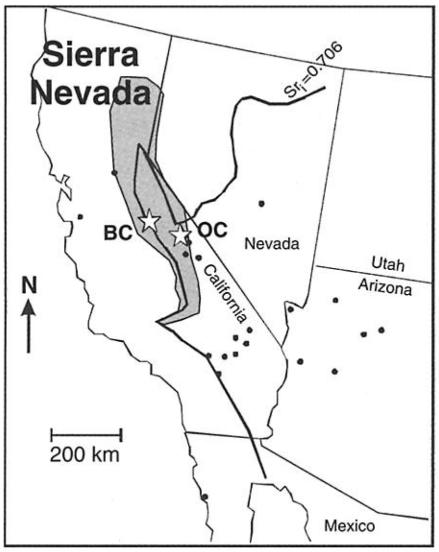

Fig. 1. Map of the Sierra Nevada showing Big Creek (BC) and Oak Creek (OC) xenolith localities. Western extent of Precambrian juvenile crust delimited by the initial $^{87}Sr/^{86}Sr$ (Sr_i) isotopic contour of 0.706 (*13*). Other xenolith localities denoted by black dots.

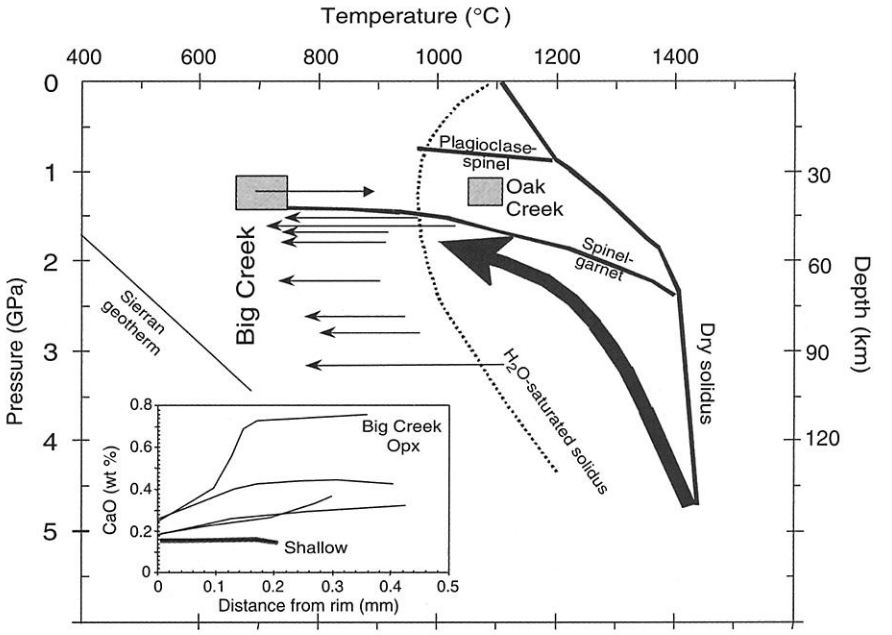

Fig. 2. Pressure-temperature (*P-T*) diagram with thermobarometric results (*28*); pressure in gigapascals. Big Creek peridotites can be divided into two groups: a deep group (>45 to 60 km), consisting of garnet and spinel peridotites, characterized by orthopyroxenes zoned from high CaO cores to low CaO rims, and a shallow group (<45 to 60 km), consisting of spinel peridotites, characterized by either homogeneous orthopyroxenes or orthopyroxenes zoned from low CaO cores to high CaO rims. The deep peridotites show cooling from temperatures >1100°C to ~750°C, whereas the shallow peridotites are cold (670° to 740°C; square) and may show heating up to 900°C. Inset shows CaO zonation in orthopyroxene grains (versus distance away from contact with clinopyroxene) in some Big Creek xenoliths (thin line, deep xenoliths; thick line, shallow xenolith). Arrows connect core to rim temperatures in the deep Big Creek xenoliths. Oak Creek peridotites are hot and homogeneous (filled square at ~1050°C). Large black arrow represents a possible *P-T* path that the deep Big Creek xenoliths may have taken in order to satisfy the high core temperatures and the high olivine Mg#, which indicate that they are residues of melting. Solidus curves and spinel-garnet transitions are from references (*27*) and (*49*). Sierran geotherm based on ~40 mW/m² surface heat flow (*50*).

peratures, as evidenced by zoned orthopyroxenes. The Sierran crust is presently ~35 km thick (*11*). If the original Sierran lithosphere was at least 100 km thick, then the lower ~60 to 85% of the original central Sierran SCLM was removed, leaving behind only a sliver of ancient mantle beneath the Moho, which experienced heating.

Removal of SCLM can be accomplished by thermal erosion associated with a rising plume head, by extensional thinning of the lithosphere (and associated mantle upwelling), or by processes related to contractional tectonics [e.g., foundering of lithosphere during thickening, peeling of lithosphere, shearing away of lithosphere during shallow subduction, or erosion of lithosphere induced by flow in the mantle wedge above a subducting slab (*1–5, 7*)]. The lack of evidence for a plume in this region of southwestern North America argues against the plume erosion model, leaving the last two mentioned as possibilities.

In principle, both extensional and contractional forms of lithospheric removal can produce the young Re-Os model ages and the thermal histories observed in the deep Big Creek xenoliths. Cessation or slowing of extension results in incorporation of asthenospheric mantle into the SCLM by conductive cooling. In the contraction-related removal hypothesis, lithosphere is removed faster than thermal reequilibration (*1–4*), and hot asthenospheric mantle, which rises to fill the region vacated by SCLM removal, cools as it impinges on the surrounding cold lithosphere. Both processes also result in melting and generation of refractory residues as asthenospheric mantle upwells adiabatically into the region of thinned lithosphere.

Determining the timing of SCLM removal would help distinguish between these processes. Extensional events in southwestern North America are recognized during two periods: mid- to latest Proterozoic continental breakup (*32*) and mid- to late Cenozoic extension in the Basin and Range (*33*). Contractional removal might occur in association with compressional deformation during the Mesozoic or low-angle subduction in the early Cenozoic (*34*).

Zoned orthopyroxenes in the central Sierran xenoliths provide an estimate of the maximum residence time of these radiogenic peridotites. Calcium diffusion length scales are 0.2 to 0.3 mm. Assuming residence temperatures of ~800°C (final equilibration temperatures based on rim-rim contacts using two-pyroxene or garnet-pyroxene thermometers), and a diffusion coefficient for Ca in orthopyroxene at 800°C of $\sim 10^{-23}$ m^2/s (*35*), the diffusion profiles would be erased within 100 to 300 Ma of their formation. This argues against a Proterozoic removal event. A minimum age of lithospheric removal can be estimated by calculating the cooling time of the new lithosphere. Assuming the lower

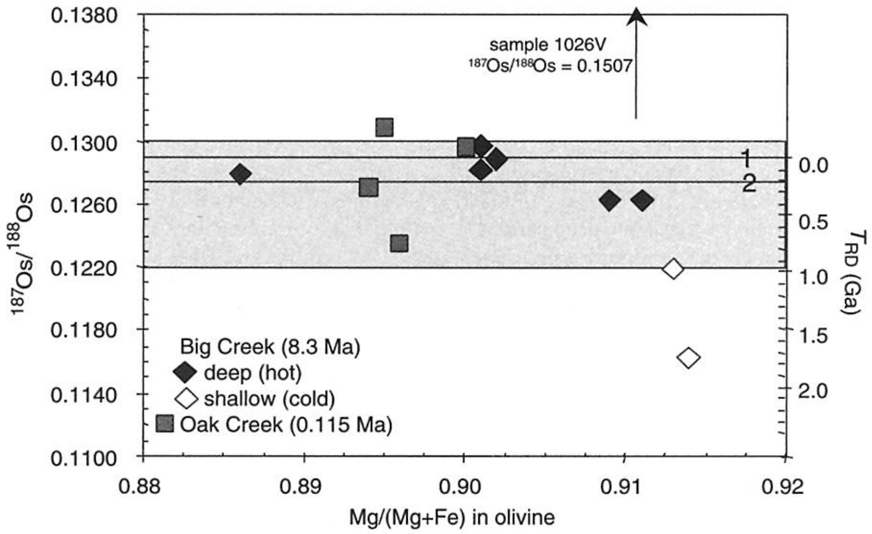

Fig. 3. ^{187}Os/^{188}Os versus olivine Mg#. Shaded field is the ^{187}Os/^{188}Os range for modern convecting mantle (*20*). Lines 1 and 2 represent different estimates of the present day ^{187}Os/^{188}Os of primitive upper mantle (*20, 22*). Right axis shows Re depletion ages (*20*). Arrow points toward an unusually radiogenic garnet-bearing spinel lherzolite from Big Creek (sample 1026V); unlike other samples, this sample contains abundant sulfides.

Table 1. Composition and characteristics of peridotite xenoliths from the Sierra Nevada. Model ages for those samples with ^{187}Os/^{188}Os > 0.129 are not given, because they bear no age significance. Re-Os data for BC77 and duplicate of 1026V were obtained at the University of Arizona; all other data obtained at Harvard University using a Finnigan Mat262.

Sample*	Rock type†	Mg# olivine‡	Mg# bulk‡	Na_2O cpx (wt %)†	Sulfur (ppm)	Pressure (GPa)	fO_2 ΔFMQ§	Re (ppb)	Os (ppb)	^{187}Re/^{188}Os	^{187}Os/^{188}Os	T_{MA} (Ga)‖	T_{RD} (Ga)¶
						Big Creek							
P1	sp lherz	0.886	0.882	0.54		<2	−0.28	0.252	3.65	0.321	0.1279 ± 4	0.7	0.16
P-2	sp harz	0.914		0.69		<2.5		0.045	3.60	0.059	0.1163 ± 3	2.1	1.80
dupl.								–	3.31	–	–	–	–
P-6	sp gt lherz	0.902	0.890	1.61	134	3.0	−0.25	–	1.21	–	0.1288 ± 3	–	0.02
dupl.								0.151	3.39	–	–	–	–
P7	sp lherz	0.901	0.895	1.35	143	<2	−1.05	0.191	4.00	0.226	0.1296 ± 9	–	–
P10	sp lherz	0.909	0.895	0.72	98	<2	0.18	0.013	3.87	0.016	0.1263 ± 3	0.40	0.387
BC98-2	sp harz	0.913	0.903	0.46		<2	−1.02	0.092	4.31	0.101	0.1219 ± 8	1.33	1.01
BC77	sp gt lherz	0.911	0.903	1.04	32	2.2		0.297	3.61	0.396	0.1263 ± 2	6.00	0.38
96D18	sp gt lherz	0.901	0.886	1.55		2.8		0.045	2.29	0.093	0.1281 ± 2	0.16	0.12
1026V	sp gt lherz	0.910	0.899	0.98	230	3.2		0.375	4.41	0.402	0.1507 ± 7	–	–
dupl.								0.348	3.76	0.447	0.1551 ± 3	–	–
						Oak Creek							
OK98-2	sp lherz	0.896		1.63		<1.5	−0.27	0.075	2.84	0.125	0.1235 ± 4	1.10	0.78
OK98-3	sp lherz	0.895	0.890	1.62	26	<1.5	−1.13	0.053	1.14	0.220	0.1309 ± 4	–	–
OK98-4	sp lherz	0.894	0.894	1.76	67	<1.5	−0.85	0.118	1.53	0.363	0.1271 ± 3	1.95	0.28
OK98-9	sp lherz	0.900		1.04		<1.5	−0.70	0.093	1.67	0.264	0.1297 ± 3	–	–

*Duplicate (dupl.) samples represent separate dissolutions. †Abbreviations: sp, spinel; lherz, lherzolite; harz, harzburgite; gt, garnet; cpx, clinopyroxene; wt %, weight %. ‡Mg# = Mg/(Mg + Fe). §fO_2 represents oxygen fugacity. ΔFMQ (log unit deviation from quartz-fayalite-magnetite buffer) for spinel peridotites (*37*), if one assumes 900°C and 2 GPa for Big Creek xenoliths and 1050°C for Oak Creek (*28*). ‖Model ages (T_{MA}) calculated with measured Re/Os and assuming present-day upper mantle with ^{187}Re/^{188}Os = 0.42 and ^{187}Os/^{188}Os = 0.129 (*21*). ¶Re depletion model ages (T_{RD}) calculated with the same mantle composition but assuming no Re present in the sample.

80% of the lithosphere cooled from ~1300°C to 800°C and a thermal diffusivity of 10^{-6} m^2/s, finite-difference models require at least a few tens of millions of years to cool to the temperatures recorded in our samples (*28*). Basin and Range extension is believed to have peaked between 10 and 15 Ma in western Nevada and eastern California (*33*). Thus, the cooling history recorded in the Big Creek xenoliths (brought up by an 8.3 Ma diatreme) cannot be related to Basin and Range extension.

The above observations are consistent with rapid SCLM removal associated with contractional tectonics. In this scenario, rapid removal of lower lithosphere (beneath 45 to 60 km) resulted in passive upwelling of asthenospheric mantle, which melted adiabatically (as evidenced by elevated olivine Mg# and low clinopyroxene Na_2O), and subsequently cooled against the remaining, cold lithosphere, which was heated slightly. The time constraints discussed above suggest that removal was associated with Mesozoic arc formation or with early Cenozoic low-angle subduction. Because low-angle Cenozoic subduction apparently resulted in the cessation of magmatism in the Sierra Nevada (*34*) and because many of the Big Creek xenoliths are residues of partial melting, it is more likely that removal occurred during the arc event. Although our observations constrain the tectonic environment for lithosphere removal, our data do not allow us to determine the precise mechanism by which removal occurred. Mesozoic removal of SCLM could have been accomplished by foundering, peeling, or active erosion associated with flow in the mantle wedge beneath the Sierran arc.

The removal of mantle lithosphere documented here was probably not accompanied by lower crustal delamination, because a thin sliver of ancient mantle is preserved beneath the Moho. This ancient mantle may be the source of the isotopically enriched Cenozoic basalts observed in the eastern Sierras, although the refractory composition of the former (which the Os systematics establish as Proterozoic in age) would argue otherwise. Alternatively, the enriched Sr and Nd isotopic signatures of these basalts could have been inherited from mantle that was overprinted by a fluid/melt derived from subducted crustal material (*36*).

Finally, mantle xenoliths from the high Sierra (Oak Creek) are hot and fertile, in contrast to the cooler and variably depleted central Sierran samples. These observations could reflect removal of SCLM from beneath the high Sierra in the Pliocene, consistent with delamination of the lower crust and SCLM in this region (*37*) or thermal erosion associated with active upwelling (*38*). Alternatively, they could reflect ancient, fertile SCLM reheated during late Cenozoic extension. The existing data do not allow us to distinguish between these possibilities.

References and Notes

1. G. A. Houseman, D. P. McKenzie, P. Molnar, *J. Geophys. Res.* **86**, 6115 (1981).
2. C. P. Conrad and P. Molnar, *Geophys. J. Int.* **129**, 95 (1997).
3. P. Bird, *J. Geophys. Res.* **84**, 7561 (1979).
4. ______, *Science* **239**, 1501 (1988).
5. D. P. McKenzie and R. K. O'Nions, *Nature* **301**, 229 (1983).
6. R. L. Rudnick, *Nature* **378**, 571 (1995), and references therein.
7. Erosion associated with flow in the mantle wedge above a subducting slab is included here.
8. R. W. Kay and S. M Kay, *Tectonophysics* **219**, 177 (1993).
9. G. Zandt and C. R. Carrigan, *Science* **261**, 460 (1993).
10. B. Wernicke *et al.*, *Science* **271**, 190 (1996).
11. S. Ruppert, M. M. Fliedner, G. Zandt, *Tectonophysics* **286**, 237 (1998).
12. M. N. Ducea and J. B. Saleeby [*J. Geophys. Res.* **101**, 8229 (1996)] suggested that the absence of garnet pyroxenite in Eastern Sierran xenolith suites reflects their loss, possibly by delamination.
13. R. W. Kistler and Z. Peterman [*Geol. Soc. Am. Bull.* **84**, 3489 (1973)] showed that the initial $^{87}Sr/^{86}Sr$ = 0.706 contour in the Sierran batholith approximates the western limit of Paleozoic miogeoclinal sediments (Fig. 1). Plutons east of the contour have $^{87}Sr/^{86}Sr > 0.706$, whereas those to the west have $^{87}Sr/^{86}Sr < 0.706$, and Nd follows suit, i.e., $\varepsilon_{Nd} < 0$ and $\varepsilon_{Nd} > 0$, respectively (*14*). Lower crustal xenoliths from late Miocene diatremes just to the east of the 0.706 contour have Sr and Nd isotopic compositions overlapping the range covered by plutons east of the 0.706 contour (*29, 40, 41*).
14. D. J. DePaolo, *Science* **209**, 684 (1980).
15. M. A. Menzies, W. P. Leeman, C. J. Hawkesworth, *Nature* **303**, 205 (1983)
16. R. F. Livaccari and F. V. Perry, *Geology* **21**, 719 (1993).
17. A. Dodson, D. J. DePaolo, B. M. Kennedy, *Geochim. Cosmochim. Acta* **62**, 3775 (1998).
18. ^{187}Re decays to ^{187}Os with a half-life of 41.6 Gy ($\lambda = 1.67 \times 10^{-11}$ per year).
19. R. J. Walker, S. B. Shirey, R. W. Carlson, F. R. Boyd, *Geochim. Cosmochim. Acta* **53**, 1583, (1989).
20. S. B. Shirey and R. J. Walker, *Annu. Rev. Earth Planet. Sci.* **26**, 423 (1998), and references therein. Assuming that modern convecting mantle consists of primitive upper mantle and depleted midocean ridge mantle (as sampled by abyssal peridotites), the $^{187}Os/^{188}Os$ of modern convecting mantle lies within the range of 0.122 to 0.130 (*39*).
21. Model ages are calculated using $^{187}Os/^{188}Os \approx 0.129$ [T. Meisel, R. J. Walker, J. W. Morgan, *Nature* **383**, 517 (1996)] and $^{187}Re/^{188}Os = 0.42$ for the present-day convecting mantle.
22. Small-scale heterogeneity, incomplete sample dissolution, recent addition of Re to the xenolith from the host basalt, and/or recent loss of Os due to decomposition of sulfides during eruption may lead to unrepresentative Re/Os ratios or change in Re/Os after melting.
23. L. Reisberg and J. P. Lorand, *Nature* **376**, 159 (1995).
24. M. R. Handler, V. C. Bennett, T. M. Esat, *Earth Planet. Sci. Lett.* **151**, 61 (1997).
25. Whole-rock powders were made in a metal-free environment using an alumina grinding mill. Samples were spiked with ^{190}Os tracer solution, calibrated accurately to within 2‰ [Q.-Z. Yin *et al.*, *Ninth Annual V. M. Goldschmidt Conference, LPI Contrib. No. 29*, 335 (1999)]. Dissolution/spike-sample equilibration was achieved in sealed glass tubes (*42*). Os was separated and purified by using solvent extraction and microdistillation, then analyzed by negative thermal ionization mass spectrometry (233/236 = 0.0002 to 0.0006, where 236 is $^{188}Os^{16}O_3^-$ and mass 233 is monitored for background for interference from $^{185}Re^{16}O_3^-$). Measured ratios were corrected for oxides ($^{17}O/^{16}O = 0.0003708$ and $^{18}O/^{16}O = 0.002045$) and for mass discrimination. Re was separated by anion-exchange and analyzed by inductively coupled plasma mass spectrometry. Os and Re processing blanks were <3 pg ($^{187}Os/^{188}Os = 0.139$) and <6 pg, respectively. External reproducibility of $^{187}Os/^{188}Os$ for ~1 ng standard was 3‰ over the course of the study.
26. F. C. W. Dodge, J. P. Lockwood, L. C. Calk, *Geol. Soc. Am. Bull.* **100**, 938 (1988).
27. A. V. Girnis and G. P. Brey, *Eur. J. Mineral.* **11**, 619 (1999).
28. Temperatures were calculated using garnet-pyroxene and Ca-in-orthopyroxene thermometers, and pressures were calculated using garnet-orthopyroxene barometers, as detailed by C.-T. Lee, R. L. Rudnick, and G. H. Brimhall Jr. (in preparation) and in (*41*). Garnet exsolution in pyroxene and spinel rimmed by garnet also suggest cooling.
29. B. Mukhopadhyay and W. I. Manton, *J. Petrol.* **35**, 1417 (1994).
30. Because most of the xenoliths are small (<6 cm diameter), whole-rock major-element analyses were not possible for all samples. We thus use the forsterite content of olivines and the Na_2O content of clinopyroxenes as measures of the degree of melt depletion.
31. An alternative interpretation, that the asthenospheric $^{187}Os/^{188}Os$ reflects addition of radiogenic Os to unradiogenic peridotites, is considered unlikely for most samples. Sulfide addition is unlikely because sulfides are exceedingly rare in the xenoliths. Moreover, variable addition of radiogenic sulfides, probably containing 1000 times more Os than the bulk peridotite (*43*) and having $^{187}Os/^{188}Os > 0.150$, should create highly variable $^{187}Os/^{188}Os$, which is not seen. We also rule out addition of radiogenic Os by aqueous fluids, as suggested for some arc peridotites (*44*) because our samples, unlike the latter, have high Os contents (1.2 to 4.3 ppb). In addition, these arc-peridotites have high oxygen fugacities (+0.5 to +1.5 log units), hydrous minerals (*45*), and are light rare-earth element–enriched. In our samples, hydrous minerals are rare (present in only two samples), spinel peridotites have oxygen fugacities between −1.13 and +0.18 log units of the quartz-fayalite-magnetite buffer (*46*), and rare-earth element patterns range from light rare-earth-depleted to only slightly enriched (Big Creek, R. Kistler, personal communication). Only sample 1026V with $^{187}Os/^{188}Os = 0.1507$ shows evidence for Os metasomatism: it contains high sulfur contents and abundant sulfides (*47*).
32. J. H. Stewart, *Geol. Soc. Am. Bull.* **83**, 1345 (1972).
33. B. Wernicke, G. J. Axen, J. K. Snow, *Geol. Soc. Am. Bull.* **100**, 1738 (1988).
34. W. R. Dickinson and W. S. Snyder, *Mem. Geol. Soc. Am.* **151**, 355 (1978).
35. Microprobe data in preparation [as in (*28*)]. Diffusion coefficients based on compilation of W. L. Griffin, D. Smith, C. G. Ryan, S. Y. O'Reilly, T. T. Win, *Can. Mineral.* **34**, 1179 (1996). Diffusion times calculated from $t = x^2/D$, where x is the diffusion distance and D is the diffusion coefficient.
36. We have not measured (and because of limited sample size, probably will not measure) the Sr and Nd isotopic composition of the Big Creek xenoliths from our collection. However, a number of published and unpublished Sr isotopic data are available to us for Big Creek (including three of our samples) and Oak Creek peridotites [(*40, 41, 48*) and R. Kistler, unpublished data]. Some of these samples have radiogenic $^{87}Sr/^{86}Sr$ and unradiogenic $^{143}Nd/^{144}Nd$ (although not all samples were analyzed for Nd), in apparent contradiction with the asthenospheric $^{187}Os/^{188}Os$ of many of the Big Creek and Oak Creek samples. However, in $^{87}Sr/^{86}Sr$ versus 1/Sr space, these peridotites define a linear trend, consistent with a Mesozoic or younger overprinting hypothesis.
37. M. Ducea and J. Saleeby, *Earth Planet. Sci. Lett.* **156**, 101 (1998).
38. M. Liu and Y. Shen, *Geology* **26**, 299 (1998).
39. J. E. Snow and L. Reisberg, *Earth Planet. Sci. Lett.* **133**, 723 (1995).
40. M. A. Domenick, R. W. Kistler, F. C. W. Dodge, M. Tatsumoto, *Geol. Soc. Am. Bull.* **94**, 713 (1983).

41. M. N. Ducea and J. B. Saleeby, *Contrib. Mineral. Petrol.* **133**, 169 (1998).
42. S. B. Shirey and R. J. Walker, *Anal. Chem.* **67**, 2136 (1995).
43. S. R. Hart and G. E. Ravizza, in *Earth Processes: Reading the Isotopic Code*, A. Basu and S. Hart, Eds., (Geophys. Monogr. Ser. 95, American Geophysical Union, Washington, DC, 1996), pp. 123–134.
44. A. D. Brandon, R. A. Creaser, S. B. Shirey, R. W. Carlson, *Science* **272**, 861 (1996).
45. A. D. Brandon and D. S. Draper, *Geochim. Cosmochim. Acta* **60**, 1739 (1996).
46. C. Ballhaus, R. F. Berry, D. H. Green, *Contrib. Mineral. Petrol.* **107**, 27 (1991).
47. J. T. Chesley, R. L. Rudnick, C.-T. Lee, *Geochim. Cosmochim. Acta* **63**, 1203 (1999).
48. B. L. Beard and A. F. Glazner, *J. Geophys. Res.* **100**, 4169 (1995).
49. D. H. Green, *Earth Planet. Sci. Lett.* **19**, 37 (1973).
50. A. H. Lachenbruch and J. H. Sass, in *The Earth's Crust: Its Nature and Physical Properties*, J. G. Heacock, Ed., (Geophys. Monogr. Ser. 625, American Geophysical Union, Washington, DC, 1977), pp. 626–675.
51. We thank P. Bird, A. Brandon, D. Coleman, M. Ducea, M. Handler, D. Lambert, S. Shirey, and four anonymous journal reviewers for helpful comments, S. Sorensen (Smithsonian Institution, P6, P7, P10, D18) and R. Kistler are thanked for lending several samples, J. Ruiz for access to the W. M. Keck Foundation laboratory at the University of Arizona, where two of the samples were analyzed, and M. Rhodes for XRF analyses. This research was supported by the NSF (EAR 9909526 to R.L.R., a graduate fellowship to C.-T.L., and EAR 9628195 and EAR9616072 to S.B.J.).

20 June 2000; accepted 13 July 2000

A High-Resolution Millennial Record of the South Asian Monsoon from Himalayan Ice Cores

L. G. Thompson,[1,2*] T. Yao,[3] E. Mosley-Thompson,[1,4] M. E. Davis,[1,2] K. A Henderson,[1,2] P.-N. Lin[1]

A high-resolution ice core record from Dasuopu, Tibet, reveals that this site is sensitive to fluctuations in the intensity of the South Asian Monsoon. Reductions in monsoonal intensity are recorded by dust and chloride concentrations. The deeper, older sections of the Dasuopu cores suggest many other periods of drought in this region, but none have been of greater intensity than the greatest recorded drought, during 1790 to 1796 A.D. of the last millennium. The 20th century increase in anthropogenic activity in India and Nepal, upwind from this site, is recorded by a doubling of chloride concentrations and a fourfold increase in dust. Like other ice cores from the Tibetan Plateau, Dasuopu suggests a large-scale, plateau-wide 20th-century warming trend that appears to be amplified at higher elevations.

The Holocene climate of the southern Tibetan Plateau has been dominated by the South Asian Monsoon in the summer and by westerly cyclonic activity in the winter. The strength of the monsoon is determined by a number of forcing mechanisms operating over a variety of time scales. Northern Hemisphere (NH) insolation has been relatively high over the past 10,000 years with correspondingly greater monsoonal activity than during the last glacial stage, when NH insolation was lower. At that time, reduced differential heating between the Indian Ocean and the Asian continent weakened the summer circulation, producing cooler, drier conditions over Asia and across the southern plateau (*1*). On shorter time scales, variations in the strength of the South Asian Monsoon have been explained by changes in internal boundary conditions, such as increasing tropical sea surface temperatures (*2*, *3*), variations in Eurasian snow cover (*4–7*), and linkages with the El Niño–Southern Oscillation (ENSO) (*8–10*). The Himalayas contain the largest volume of ice outside the polar regions, and the meltwater from its glaciers form the headwaters of such important rivers as the Indus and the Ganges. Here, we examine the variability of the South Asian Monsoon as recovered from Himalayan ice cores.

In 1997, three ice cores were recovered from the Dasuopu glacier (28°23′N, 85°43′E) with the use of an electromechanical drill in dry holes (Fig. 1). The first core (C1) was 159.9 m long and was drilled at 7000 m above sea level (a.s.l.) down the flow line from the top of the col, and two cores (C2 and C3), 149.2 and 167.7 m long, respectively, were drilled to bedrock 100 m apart on the col at 7200 m a.s.l. Visible stratigraphy showed no hiatus features in any of the cores. C2 was brought (in a frozen state) to the Lanzhou Institute of Glaciology and Geocryology (LIGG), C3 was brought (also frozen) to the Byrd Polar Research Center, and C1 was split between the two institutes. All cores were analyzed over their entire lengths for oxygen isotopic ratio ($\delta^{18}O$), chemical composition, and dust concentration. Most of the results presented here are from C3, which was cut into 6903 samples for both $\delta^{18}O$ and hydrogen isotopes (δD) and into 6419 samples each for insoluble dust, chloride (Cl^-), sulfate (SO_4^{2-}), and nitrate (NO_3^-) analyses. Borehole temperatures were −16.0°C at 10 m depth and −13.8°C at the ice-bedrock contact, demonstrating that the Dasuopu glacier is frozen to its bed.

In general, the bulk of the annual precipitation received in the Himalayas arrives during the summer monsoon season. At the col of Dasuopu, the average annual net balance is ~1000 mm water equivalent (w.e.) as determined by snow pit and shallow core studies and by the measurement of a 12-stake accumulation network established during a reconnaissance survey in July 1996. The high annual accumulation allows preservation of distinct seasonal cycles, particularly in $\delta^{18}O$, dust, and NO_3^-, which make it possible to reconstruct an annual record for the last 560 years from the upper 87% of C3. As in tropical cores from the Andes (*11–15*), $\delta^{18}O$ enrichment and high aerosol concentrations occur in the winter dry season, and $\delta^{18}O$ depletion and lower aerosol concentrations occur during the wet summer season. The annual layer counting was verified at 42.2 m by the location of a 1963 beta radioactivity horizon produced by the 1962 atmospheric thermonuclear tests in the Arctic. Surprisingly, despite the proximity of the Himalayas to the volcanically active Indonesian archipelago, no obvious traces of historically known eruptions (e.g., Krakatau and Tambora) were found. Based on the dust and $\delta^{18}O$ stratigraphy, C3 was annually dated to 1440 A.D. ± 3 years at a depth of 145.4 m. Below this horizon, layer thinning made annual resolution of the records impossible. Therefore from 1439 to 1000 A.D. (145.4 to 154.6 m), the time scale was determined by extrapolating the depth-age relation established for the upper 145 m and by assuming a constant annual accumulation rate. Thus, for the lower section only decadal averages were calculated with

[1]Byrd Polar Research Center, The Ohio State University, Columbus, OH 43210, USA. [2]Cold and Arid Regions Environmental and Engineering Institute, Chinese Academy of Sciences, Lanzhou China. [3]Department of Geological Sciences, [4]Department of Geography, The Ohio State University, Columbus, OH 43210, USA.

*To whom correspondence should be addressed. E-mail: thompson.3@osu.edu